The Plant Cell, Vol. 26: 4834–4842, December 2014, www.plantcell.org

The *Arabidopsis* Cellulose Synthase Complex: A Proposed Hexamer of CESA Trimers in an Equimolar Stoichiometry[W]

Joseph L. Hill, Jr., Mustafa B. Hammudi, and Ming Tien[1]

Department of Biochemistry and Molecular Biology, Pennsylvania State University, University Park, Pennsylvania 16802

Cellulose is the most abundant renewable polymer on Earth and a major component of the plant cell wall. In vascular plants, cellulose synthesis is catalyzed by a large, plasma membrane-localized cellulose synthase complex (CSC), visualized as a hexameric rosette structure. Three unique cellulose synthase (CESA) isoforms are required for CSC assembly and function. However, elucidation of either the number or stoichiometry of CESAs within the CSC has remained elusive. In this study, we show a 1:1:1 stoichiometry between the three *Arabidopsis thaliana* secondary cell wall isozymes: CESA4, CESA7, and CESA8. This ratio was determined utilizing a simple but elegant method of quantitative immunoblotting using isoform-specific antibodies and ^{35}S-labeled protein standards for each CESA. Additionally, the observed equimolar stoichiometry was found to be fixed along the axis of the stem, which represents a developmental gradient. Our results complement recent spectroscopic analyses pointing toward an 18-chain cellulose microfibril. Taken together, we propose that the CSC is composed of a hexamer of catalytically active CESA trimers, with each CESA in equimolar amounts. This finding is a crucial advance in understanding how CESAs integrate to form higher order complexes, which is a key determinate of cellulose microfibril and cell wall properties.

INTRODUCTION

The ability of cellulose to serve as a structural polymer in the secondary cell wall of plants is due, in part, to its potential for high crystallinity, which results from its extensive interchain and intrachain hydrogen bonding network (Visakh and Thomas, 2010). The individual glucose monomers of cellulose are enzymatically linked into β-1,4-glucan chains prior to the crystallization process (Morgan et al., 2013). While crystalline properties of cellulose are essential for upright plant growth, this crystallinity is one obstacle in efficiently utilizing lignocellulosic material for bioenergy purposes. Because cellulose crystallinity is highly dependent upon interchain interaction, the proximity and number of adjacent chains are thought to greatly affect its physical properties. These parameters are ultimately defined by the plasma membrane-embedded cellulose synthase complex (CSC), where cellulose biosynthesis originates.

The CSCs of vascular plants were first visualized through freeze-fracture transmission electron microscopy as hexameric rosette structures containing cellulose synthase (CESA) proteins (Kimura et al., 1999). Genetic and biochemical evidence has shown that three unique CESA isoforms are required for CSC function and that separate CSCs are involved in primary cell wall (PCW) and secondary cell wall (SCW) cellulose biosynthesis. In *Arabidopsis thaliana*, CESA1, CESA3, and CESA6 are required for PCW cellulose biosynthesis, while CESA4, CESA7, and CESA8 are required during SCW development. The remaining CESAs (CESA2, CESA5, CESA9, and CESA10) are involved in tissue-specific processes and are partially redundant with CESA6 (Gardiner et al., 2003; Taylor et al., 2003; Persson et al., 2007). Until recently, the only proteins identified as integral to the CSC were CESAs (Kimura et al., 1999), but the cellulase KORRIGAN has now been implicated as an integral component of the CSC (Vain et al., 2014).

To further understand the mechanism of cellulose biosynthesis, a number of laboratories are attempting to identify the full suite of proteins integral to the complex and elucidate the stoichiometry, number, and arrangement of CESAs within the CSC (Gu et al., 2010; Guerriero et al., 2010; Bashline et al., 2013; Olek et al., 2014). To account for the alternating glucose conformers of cellulose, a previous model suggested that two CESAs were required to synthesize a single glucan chain (Carpita, 2011). However, the crystal structure of a bacterial cellulose synthase has shown that a single synthase is sufficient for catalysis (Morgan et al., 2013). Assuming that each CESA of the CSC is active and that each active site produces a single β-1,4-glucan chain, then measurements of cellulose microfibril diameter can, and have, been used to estimate the number of active sites within the CSC. One such estimation suggested that CSCs contain 36 CESAs (Herth, 1983). This 36-mer hypothesis was perpetuated through various CSC models, with CESAs in a 1:2:3 (Doblin et al., 2002) or 1:1:1 (Taylor, 2008; Timmers et al., 2009) stoichiometry. However, the idea of 36 glucan chains per microfibril has been challenged many times in the past (Chanzy et al., 1978, 1979; Ha et al., 1998; Thimm et al., 2002; Kennedy et al., 2007) and by several more recent studies, utilizing multiple-technique measurements of microfibril size and data fitting, estimating 18 to 24 glucan chains per microfibril (Fernandes et al., 2011; Newman et al., 2013; Thomas et al., 2013). These data suggest that the CSC may constitute as little as 18 CESAs. However, this represents the lower limit of CESAs within a CSC,

[1] Address correspondence to mxt3@psu.edu.
The author responsible for distribution of materials integral to the findings presented in this article in accordance with the policy described in the Instructions for Authors (www.plantcell.org) is: Ming Tien (mxt3@psu.edu).
[W] Online version contains Web-only data.
www.plantcell.org/cgi/doi/10.1105/tpc.114.131193

as the CSC could function with only a subset of CESAs active at any given time. The traditional upper limit of 36 CESAs per CSC has never been precisely defined. This could be derived from modeling CESA transmembrane regions and fitting to rosette size measurements from freeze-fracture transmission electron microscopy, as suggested by Newman et al. (2013). Experiments using blue native PAGE (BN-PAGE) have also supported a 36-CESA CSC model. Immunoblot visualization of BN-PAGE gels containing PCW and SCW CESAs reveal protein bands of 700 to 840 kD (Wang et al., 2008; Atanassov et al., 2009). This molecular mass range is consistent with a hexamer of CESAs, which has been assumed to further assemble into a 36-mer.

As a first step toward characterizing the CSC, this study determines the stoichiometry of the CESAs within the SCW CSC. Our results clearly indicate an equimolar stoichiometry between CESA4, CESA7, and CESA8. Taking this stoichiometry and a body of previous evidence into account, we comment on the plausibility of several models of the CSC. We propose a model of a hexamer of catalytically active CESA trimers in a 1:1:1 stoichiometry as a likely model for the CSC.

RESULTS

Preparation of Isoform-Specific CESA Antibodies

To conduct quantitative immunoblotting, it was necessary to generate specific antibodies to each CESA under study. However, *Arabidopsis* CESAs have an average sequence identity of 69% (61 to 91%), with nonhomologous sequences located predominantly in two regions (Supplemental Figure 1). Accordingly, unique peptide sequences for CESA1, CESA4, CESA7, and CESA8 were identified (Supplemental Table 1) and synthesized for use as antigens. Where possible, multiple peptide antigens were used to ensure the successful generation of a specific polyclonal antibody. This resulted in the creation of several antibody populations (denoted with a decimal number), which could be separated by their affinity to a specific antigen peptide. Immunoblot analysis of each antibody population revealed a range of sensitivity and specificity, as shown in Figure 1. Each antibody population (except anti-CESA4.2) exhibited strong immunodetection of an ~120-kD band corresponding to CESA (Figure 1, arrows). This band was absent from protein extracts of the corresponding knockout line, confirming isoform specificity. Additional signals were observed at various molecular masses; each of these bands was also observed in the corresponding knockout line, signifying that they arose from cross-reactions to proteins other than CESA. Based on specificity and sensitivity, anti-CESA4.3, anti-CESA7.3, and anti-CESA8.2 were used for this study.

A *cesa1* knockout was unavailable to test the specificity of anti-CESA1, as available T-DNA insertions have been shown to be gametophytic lethal (Persson et al., 2007). Instead, heterologously expressed CESAs were used to show the specificity of the anti-CESA1 antibody and allow further confirmation of SCW CESA antibody specificity (Figure 2). These data show that the antibodies generated against CESA1, CESA4, CESA7, and CESA8 are suitably specific to their designated CESAs for both general detection and quantitative immunoblotting.

Heterologous Expression of Full-Length CESA in Vitro

Quantitative immunoblotting necessitates a protein standard that can be used for immunoblot analysis and be quantified by some separate means. Heterologous expression of full-length CESAs in *Escherichia coli*, even in inclusion bodies, was

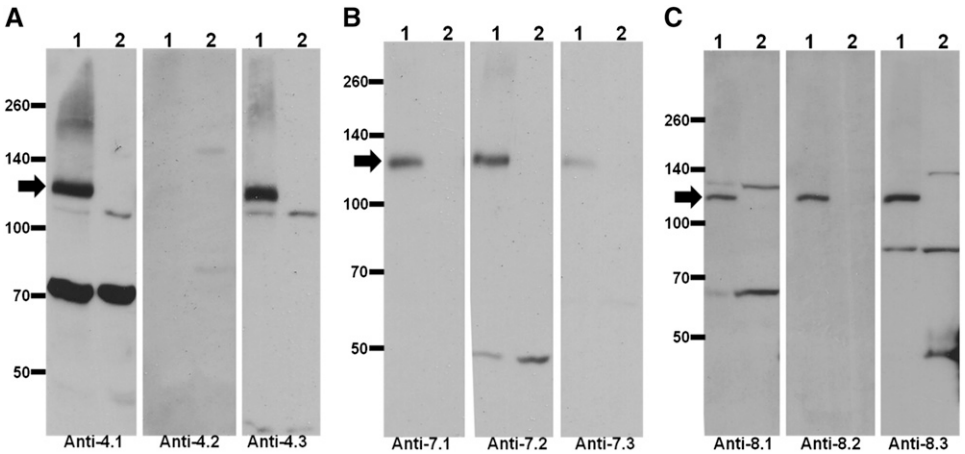

Figure 1. Specificity of Antibody Populations.

Equal amounts of protein from wild-type and *cesa* knockout stems were analyzed by immunoblot with affinity-purified populations of antibodies. Arrows indicate bands corresponding to CESA. Signals corresponding to other bands are cross-reactions with non-CESA proteins. Anti-CESA4.3, anti-CESA7.3, and anti-CESA8.2 were chosen for further use.

(A) Antibodies to CESA4. Lane 1, the wild type; lane 2, *cesa4*.

(B) Antibodies to CESA7. Lane 1, the wild type; lane 2, *cesa7*.

(C) Antibodies to CESA8. Lane 1, the wild type; lane 2, *cesa8*.

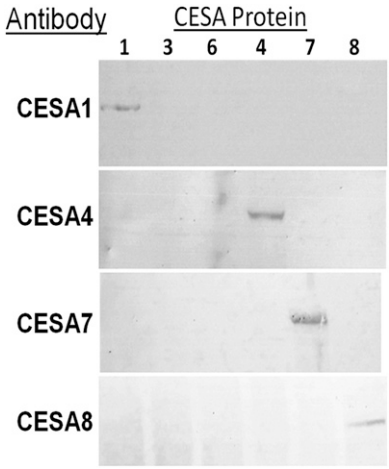

Figure 2. Antibody Specificity by Analysis of Heterologously Expressed CESAs.

The most abundant *Arabidopsis* CESAs (CESA1, CESA3, CESA6, CESA4, CESA7, and CESA8) were heterologously expressed in a cell-free wheat germ coupled transcription/translation system. Four identical SDS-PAGE gels were prepared and probed with different CESA antibodies. Immunodetection occurred only with the intended CESA isoform (i.e., anti-CESA1 detected CESA1 and failed to react with CESA3, CESA6, CESA4, CESA7, and CESA8).

problematic (data not shown). However, full-length CESA protein expression was achieved in a wheat germ (*Triticum aestivum*) coupled transcription/translation system (Promega). Because this system involves the addition of individual amino acids (for tRNAs), incorporation of [^{35}S]methionine could be used to radiolabel the CESA protein standards. This provided for a robust means for quantifying the amount of protein present through liquid scintillation counting. The major product synthesized by the in vitro reaction was full-length CESA protein as visualized by immunoblot and autoradiogram (Figure 3).

Quantification of CESA4, CESA7, and CESA8 by Immunoblotting Reveals Equimolar Stoichiometry

Quantification by immunoblot involves generating a standard curve to correlate band intensity to the absolute molar amount of protein. Varying quantities of the ^{35}S-labeled CESA standards were subjected to immunoblot analysis alongside a series of *Arabidopsis* stem protein extracts. Following the quantification of immunoblot band intensity by ImageJ (Schneider et al., 2012), the mole quantities of [^{35}S]methionine-containing CESA standards on the nitrocellulose membrane were measured by liquid scintillation counting. This calculation is made possible by knowing the methionine content of each CESA, the specific activity of the [^{35}S]methionine, and use of an internal standard. Band intensity measurements, along with protein quantification by scintillation counting, provided the data for a standard curve (Figures 4A to 4F). Results from a series of four immunoblots per CESA, each with its own standard curve (average r^2 value of 0.968), yielded the following quantities: 2.3 $\pm$ 0.3 (CESA4), 2.10 $\pm$ 0.36 (CESA7), and 2.02 $\pm$ 0.22 (CESA8) amol/μg total protein (Figure 4G). These results indicate that there is an equimolar stoichiometry between CESA4, CESA7, and CESA8 in the measured sample. This represents the whole-cell stoichiometry, as it was measured from a total protein extract, rather than purified CSCs. If most or all of the CESA proteins were contained within CSCs, then it would follow that the whole-cell stoichiometry accurately reflects the stoichiometry within the CSC.

Incomplete CSCs Are Unstable in Vivo

As a proxy measure for levels of CESAs outside CSCs, the levels of each CESA protein in SCW *cesa* knockout lines were assessed by immunoblot. As shown in Figure 5, in any given *cesa* null background, very low (if any) levels were observed for remaining interacting partner CESAs (i.e., loss of one isoform results in the near elimination of the remaining two). As a control, in these knockout lines, the protein level of CESA1 was also examined. The reduction in protein levels observed with SCW CESAs was not mimicked by CESA1, which exists in the separate and distinct CSC, and thus should not be directly affected (Figure 5).

These results suggest that the absence of a single CESA creates incomplete CSCs, which are not stable in vivo. This is consistent with rapid CESA assembly occurring, as intermediate complexes would not be stable. Following this line of logic, our data are consistent with few CESAs existing outside of CSCs, as independent CESAs or partial CSCs fail to accumulate in vivo (Figure 5). The requirement of CESAs to be within a CSC for stability implies that the measure of whole-cell CESA stoichiometry is representative of the stoichiometry within the CSC.

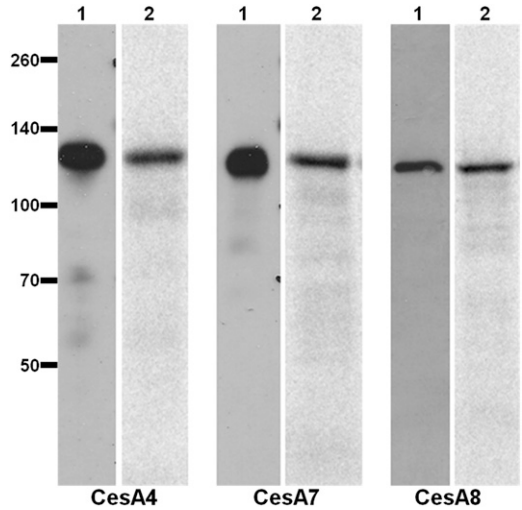

Figure 3. Heterologous Expression of CESAs in Vitro.

CESA4, CESA7, and CESA8 were heterologously expressed in a wheat germ cell-free coupled transcription/translation system in vitro and labeled with [^{35}S]methionine. The major product was full-length CESA, which was detectable by immunoblot (lane 1) and autoradiogram (lane 2).

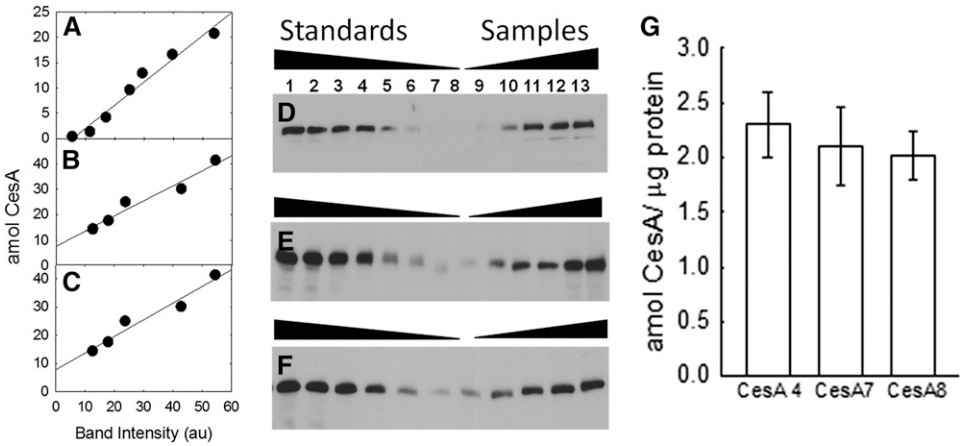

Figure 4. Quantitative Immunoblotting of CESA4, CESA7, and CESA8 Displays a 1:1:1 Stoichiometry.

(A) to **(C)** Representative standard curves for CESA4, CESA7, and CESA8. au, arbitrary units.
(D) to **(F)** Immunoblots corresponding to the standard curves shown in **(A)** to **(C)**. Lanes 1 to 7, ^{35}S-labeled, heterologously expressed CESA, decreasing amounts; lanes 8 to 13, increasing amounts of total protein from *Arabidopsis* stem (3, 4.5, 6, 9, 12, and 15 µg).
(G) Calculated average concentration of each CESA with SD (n = 4 blots and n = 18 [CESA4], 20 [CESA7], and 22 [CESA8] points). There is no significant difference in CESA amount, signifying a 1:1:1 stoichiometry.

SCW CESA Stoichiometry Is Fixed through Stem Development

The span of the stem, from the base to the apex, represents a developmental gradient of SCW (base) to PCW (apex). Cells that undergo SCW biosynthesis have to transition from PCW biosynthesis, representing a stage where PCW CSCs could coexist with those of the SCW. This opens the possibility that CESAs from canonically different CSCs could mix, a hypothesis supported by promoter-swap studies demonstrating the ability for CESA1 to partially complement the *cesa8* null allele (Carroll et al., 2012; Li et al., 2013). If significant mixing were to occur under native conditions, it would likely alter the whole-cell stoichiometry of CESA4, CESA7, and CESA8. Additionally, stoichiometric modulation represents a potential mechanism for the plant to change cellulose microfibril properties during different developmental stages.

To test each of these hypotheses, *Arabidopsis* stems were divided into nine equal sections, each representing 10% of the total stem length (5 to 95%), as measured from the stem base. Immunoblot analysis was then performed on each section (Figure 6). Intensity values for each CESA were normalized to the level measured in the 25 to 35% section. A tight correlation between the protein levels of CESA4, CESA7, and CESA8 throughout all stem sections was revealed by this analysis. This indicates a consistent stoichiometry between these CESAs through various developmental stages. As a control, protein levels of a PCW CESA (CESA1) were also measured. Levels of CESA1 protein exhibit a correlation to SCW CESAs within some regions of the stem but show significant deviation in other regions (Figure 6). This indicates that the stoichiometry of CESA1 is not linked to that of the SCW CESAs. These results suggest that mixing between PCW and SCW does not occur to a significant extent and that the whole-cell stoichiometry between SCW CESAs is fixed throughout development. Furthermore, a fixed stoichiometry is also consistent with whole-cell stoichiometry being representative of CESA stoichiometry within the CSC.

DISCUSSION

Plant-based celluloses exhibit unique properties that both support anisotropic cell growth and inhibit degradation for bioenergy applications. These properties are thought to be derived from the unique rosette structure of the CSC, which is vastly different from the observed linear arrangement of bacterial cellulose synthases (Brown et al., 1976). Here, we define the stoichiometry of *Arabidopsis* SCW CESA4, CESA7, and CESA8 and comment on possible models for the rosette CSC.

CESA Stoichiometry Is 1:1:1 in SCW CSCs

Despite over a decade of research, limited information was available on the composition of the CSC. Initially, CSC models

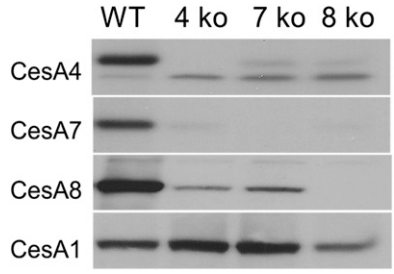

Figure 5. Immunoblot Analysis of *cesa* Knockout Lines.

Equal amounts (20 µg) of protein from the wild type and three *cesa* knockout (ko) lines were separated by SDS-PAGE and immunoblotted against CESA4, CESA7, CESA8, and CESA1 (as specified). Each knockout line shows elimination of that CESA as well as a severe reduction in the interacting partner CESAs. By contrast, levels of CESA1 remain relatively constant.

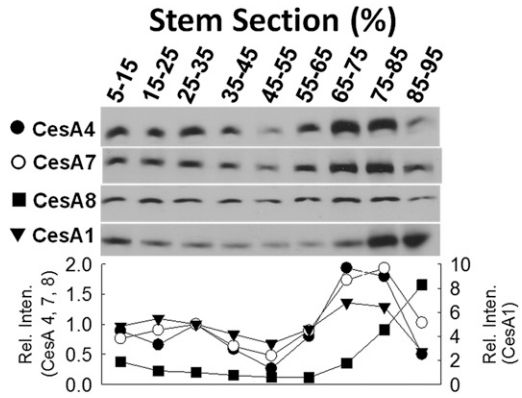

Figure 6. Immunoblot Analysis of *Arabidopsis* Stem Sections.

Equal amounts (30 μg*) of protein from sections of wild-type stem were immunoblotted against CESA4, CESA7, CESA8, and CESA1. The stem section designation is shown above the blots, while the CESA antibody used is shown to the left of the blots. Immunoblot intensity values were normalized to the 35 to 45% section and are plotted at bottom. The levels of CESA4 (closed circles), CESA7 (open circles), and CESA8 (closed triangles) show a close correlation along the entire stem, with maximal CESA levels in the sections representing 65 to 85% of the stem length as measured from the stem base. While CESA1 (closed squares) follows SCW CESA levels from 15 to 75%, indicating a consistent ratio at those points, there is a significant deviation at both the distal and apical regions of the stem. *Fifteen micrograms of sample was used for the 85 to 95% section probed for CESA1, so measured intensity was doubled.

were based solely on freeze-fracture transmission electron microscopy images showing a hexameric rosette containing CESA (Kimura et al., 1999). Research in recent years has provided additional information on the nature of the CSC but has been unable to provide an unequivocal CSC model. Studies from a number of laboratories have shown, through genetic evidence, that the CSC is composed of multiple CESA isoforms (Doblin et al., 2002; Taylor, 2008; Timmers et al., 2009; Guerriero et al., 2010). Brown et al. (2005) quantified *CESA7* and *CESA8* transcript levels, showing that *CESA7* is expressed at more than twice the level of *CESA8* in all tissues tested, suggesting an unequal stoichiometry. Other workers investigated interaction between CESAs by pair-wise yeast-two hybrid and bimolecular fluorescence assays (Desprez et al., 2007; Timmers et al., 2009; Carroll et al., 2012). In limited biochemical characterization, CESA complexes could be separated and observed by immunodetection with BN-PAGE (Wang et al., 2008; Atanassov et al., 2009). Additionally, the SCW CESAs were purified by a tandem affinity chromatography procedure, but identical gel mobility prevented the elucidation of their stoichiometry, and particles were too heterogeneous for structural determination by cryotransmission electron microscopy (Atanassov et al., 2009).

While our understanding of cellulose biosynthesis incrementally increased with the above studies, the data were often conflicting or incomplete, being unable to distinguish between hypotheses of a 1:1:1 or 1:2:3 CESA stoichiometry. Our results provide data on the stoichiometry of the three CESA isoforms of the SCW CSC, indicating a 1:1:1 stoichiometry, representing a key step in understanding the assembly of CESAs into the CSC.

The Organization of CESAs within the CSC

A high degree of promiscuity in CESA-CESA interactions was observed in pair-wise yeast two-hybrid and bimolecular fluorescence assays, where only a few CESA pairs failed to interact (Desprez et al., 2007; Timmers et al., 2009; Carroll et al., 2012). However, a more recent yeast two-hybrid study was able to observe the previously failed CESA-CESA interactions while simultaneously being unable to reproduce some of the prior results (Li et al., 2013). Taken at face value, this implies a high promiscuity for CESA-CESA interactions, providing a somewhat fluid model for CSC composition where the CSC could be of heterogeneous composition. However, yeast two-hybrid results need to be interpreted conservatively, as both false-positive and false-negative results are common (Li et al., 2013). Additionally, these studies are pair-wise in nature, lacking the essential third CESA subunit, which could explain the observed lack of specificity in CESA-CESA interactions. Thus, it is more likely that CESAs form very specific interactions in vivo, rather than with the promiscuity observed in vitro. This is supported by in planta experiments, which show that a CESA from each class is required for CSC function (Carroll and Specht, 2011; Carroll et al., 2012). Furthermore, the tight adherence to a protein level pattern along the developmental axis of the stem reveals that SCW CESA stoichiometry is fixed in *Arabidopsis* (Figure 6). A specific organization of CESAs within the CSC presents a convenient mechanism to produce this observed regulation of stoichiometry.

Other evidence for specific CESA interactions or positioning comes from an analysis of SCW *cesa* knockout lines. Previously, Ha et al. (2002) extensively analyzed the cell wall of the *cesa7* knockout line *irx3-1* (Landsberg *erecta* background) to determine the repercussions of CESA7 protein absence. These workers used Fourier transform infrared spectroscopy, NMR, and chemical analysis of isolated SCW material and found that, while the majority of wall polymers were relatively unaffected, cellulose was almost completely absent. Furthermore, they concluded that the small amount of observed cellulose originated from primary cell walls (Ha et al., 2002). This is corroborated by cellulose content analysis of the three SCW *cesa* knockouts used in this study, which have ~10% crystalline cellulose (Carroll et al., 2012). It is presumed that the cellulose measured in these lines also originates from the primary cell wall. Additionally, double knockouts of SCW CESAs show no additional mutant phenotype (Carroll and Specht, 2011). These data corroborate our protein level data, which show the absence of one CESA resulting in the concurrent loss of partner CESAs (Figure 5). Together, these observations are consistent with the entire CSC functionality being compromised with the loss of any one CESA. This, in turn, suggests that the fundamental unit for cellulose biosynthesis is a CESA trimer formed by a specific set of interactions. Elucidation of these interactions may be achieved by expanding upon previous in planta studies using chimeric CESAs (Wang et al., 2006a).

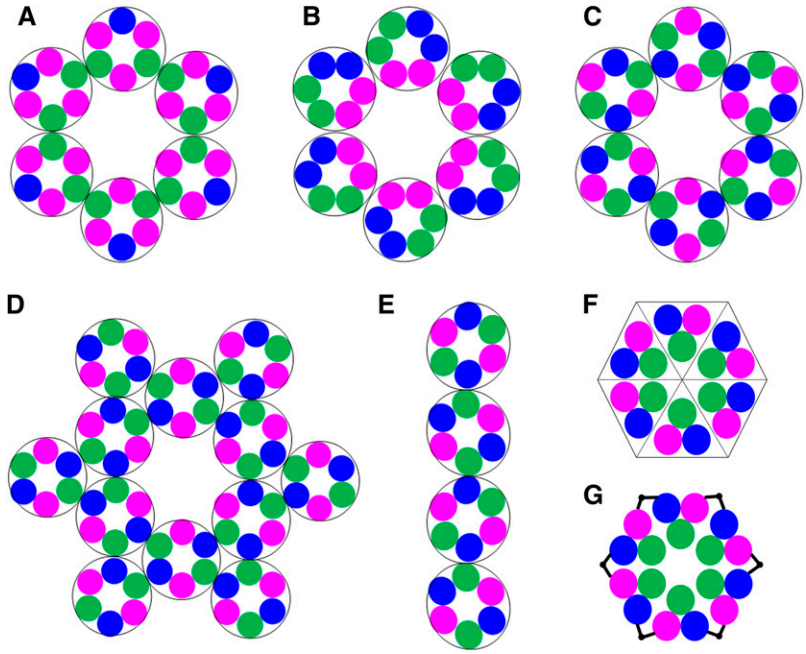

Figure 7. Models of the CSC Rosette.

Each colored circle represents one of three CESA isoforms.
(A) The hexamer of hexamers model in a 1:2:3 stoichiometry.
(B) to (**G**) Possible complexes formed with the 1:1:1 stoichiometry.
(B) Pairs of CESAs in homodimers as the fundamental unit, resulting in inconsistent protein-protein interactions.
(C) and **(D)** A hexamer of hexamers is shown where protein-protein contacts are consistent throughout **(C)**. However, as shown in **(D)**, this model can yield higher ordered CSCs wherein additional lobes are added to the rosette shown in **(C)**.
(E) A linear complex also can be formed with the green-to-blue contacts.
(F) The hexamer of trimers rosette model. Protein contacts are consistent and the rosette is self-contained.
(G) A possible mechanism for rosette assembly wherein adjacent trimers oligomerize through their N-terminal domains (black bars).

A Hexamer of CESA Trimers as a Likely Model for the CSC

Although it is often noted that the CSC is composed of 36 CESAs, this number was adopted with limited evidence (mainly based on the size of CSC rosette lobes) and then perpetuated through the years (Herth, 1983; Doblin et al., 2002). Perhaps the strongest evidence pointing toward a 36-CESA CSC comes from BN-PAGE experiments. Using immunoblotting with CESA antibodies to PCW and SCW CESAs, protein bands of 700 to 840 kD were visualized (Wang et al., 2008; Atanassov et al., 2009). Without any other data on the nature of the complex, this was assigned to be a hexamer of CESAs. By extension, it was then proposed that further assembly would yield 36-mers. This interpretation, however, has it caveats. It assumes that migration of the putative hexamer in BN-PAGE accurately correlates with migration of the soluble molecular mass standards that were used. Wittig et al. (2010), who pioneered the use of BN-PAGE, have advised against employing these commonly used soluble molecular mass standards when analyzing membrane proteins. Although sometimes accurate, they have found that various conditions can lead to large discrepancies between the behavior of soluble and membrane proteins (Wittig et al., 2010). Taking this issue into consideration, it is more suitable to view molecular masses obtained by BN-PAGE as an approximation of the upper limit rather than a strictly accurate measure of the number of CESAs present.

Bringing the iconic 36 glucan chains per microfibril into question are studies on the size of a cellulose microfibril, which, in turn, informs the number of catalytically active CESAs in the CSC. Most recently, a series of studies on both PCW and SCW microfibrils from various organisms using NMR, wide-angle x-ray scattering, small-angle neutron scattering, and computer modeling are best interpreted by microfibrils being composed of 18 or 24 glucan chains (Fernandes et al., 2011; Newman et al., 2013; Thomas et al., 2013). These results would require either a CSC composed of 18 to 24 CESAs or a larger CSC model where only 18 to 24 of the CESAs are active at any given time.

To comment on the number of CESAs within a CSC, we propose a series of reasonable rules: (1) the CSC rosette is composed of six lobes (Mueller and Brown, 1980); (2) the CSC is composed of three different CESA isoforms (Taylor et al., 2003); (3) proteins are chiral in nature, and as such, protein-protein contacts must be consistent; and (4) the number of cellulose chains (or CESA number) must be divisible by six (rosette), and when divided by six, the resultant number (which yields the number of isoforms within each lobe) must be divisible by 3 (for the three CESA isoforms). Rule 4 is a consequence of rules

1 and 2 and carries the assumption that all CESAs are active at the same time. While only CESA-CESA interactions are considered here, these rules are consistent with the incorporation of other proteins, such as KORRIGAN (i.e., the rules should not change even if other proteins are part of the complex). Seven possible models for the CSC are shown in Figure 7. The 1:2:3 model with 36 subunits shown in Figure 7A can be eliminated based on rule 3 above (e.g., the green isoform is either sandwiched between two magenta isoforms or a blue and a green isoform; this cannot be avoided). Figure 7B is the result of using homodimers as the fundamental building block in a 1:1:1 stoichiometry, which also has inconsistent protein-protein interactions. With an equimolar stoichiometry, models containing chain number (or subunit number) divisible by six would be 36, 24, 18, or 12. The 24-subunit (and 12-subunit) model can be eliminated because it violates rule 4 above and would violate rule 3 with either a 1:2:3 or 1:1:1 stoichiometry. The 36- and 18-subunit models are the only two remaining. Besides being too large to fit the spectroscopic data, the 36-CESA model (of equimolar stoichiometry), as clearly pointed out by Newman et al. (2013), cannot stop at a CSC containing precisely 36 CESAs. This is illustrated in Figure 7D, where the six lobes are added to the core shown in Figure 7C or a linear complex arrangement could be formed (Figure 7E). In the 18-CESA model (Figure 7F), increased growth of the complex cannot occur. Together, these findings support a model of the CSC that contains 18 catalytically active CESAs to form an 18-glucan chain microfibril; however, there are still many unknown questions regarding the composition of the CSC.

A recent report studying heterologously expressed truncated CESA catalytic domains concluded that the basic building block of CSC is the CESA dimer (Olek et al., 2014). While these results appear to contradict our findings here, in actuality, the two systems are very different. Their results accurately reflect the behavior of a truncated (catalytically inactive) protein, outside of the context of the entire polypeptide, and, most importantly, studied in isolation rather than with its partner CESA proteins. In contrast with Olek et al. (2014), our results are most consistent with a heterotrimer as the fundamental unit. If dimers were indeed the building blocks, they would likely be stable in planta. This is contrary to our observations that CESAs exhibit an "all-or-nothing" behavior, where the loss of any one isoform compromises the integrity of the entire CSC (Ha et al., 2002; Figure 5). Additionally, the use of a dimer as the fundamental unit only allows for the 36-CESA model of the CSC (Figure 7B). While this seems to allow for an elegant mechanism for oligomerization wherein the catalytic domains form dimers, leaving the N termini free to assemble the dimers into a hexamer (Carpita, 2011), in this simplified model, this requires the use of all catalytic and N-terminal domains to form the hexamer rather than the higher order 36-mer structure. In a model with a heterotrimeric base unit (formed by a three-way catalytic domain interaction), the N termini are then free to form the higher order structure of an 18-mer, as illustrated in Figure 7G. Additionally, only two of three N termini are strictly required, leaving the third free for additional interactions.

We can combine previous spectroscopic measurements of the cellulose microfibril and our stoichiometry results to formulate a model of the CSC. Although several assumptions are required, these data point toward a CSC made from a hexamer of equimolar stoichiometry, with catalytically active CESA trimers that synthesize an 18-glucan chain cellulose microfibril. These results further our understanding of CSC assembly from CESAs, aiding in efforts to model the CSC (Sethaphong et al., 2013) and in elucidating the process that produces the unique properties of the cellulose microfibril and plant cell wall.

METHODS

CESA Antibody Synthesis

Peptides (Supplemental Table 1 and Supplemental Figure 1) were designed to match unique sections of the CESA hypervariable regions, chemically synthesized, and then injected into New Zealand White rabbits to generate polyclonal antibodies (Covance). For CESA4, CESA7, and CESA8, a mixture of three peptide antigens was injected into a single rabbit (i.e., peptides CESA4.1, CESA4.2, and CESA4.3 were collectively injected into a single rabbit). For CESA1, only a single peptide antigen was synthesized and injected. Antibodies were purified from total serum by their affinity to a specific peptide antigen using the SulfoLink Immobilization Kit for Peptides (Thermo) according to the manufacturer's instructions. Antibody specificity was assayed by probing samples of wild-type Columbia *Arabidopsis thaliana*, *cesa* knockout lines, and CESAs heterologously expressed in the cell-free wheat germ (*Triticum aestivum*) system (Promega). Antibodies purified for their affinity to the CESA4.3, CESA7.3, and CESA8.2 peptides were used throughout this study, as they showed the least cross-reactivity with non-CESA proteins.

Heterologous Expression of CESA in a Wheat Germ Cell-Free Coupled Transcription/Translation System

The cDNAs of CESA4, CESA7, and CESA8 were amplified by PCR with the primers shown in Supplemental Table 2. PCR-amplified products were cloned into *Kpn*I- and *Asi*SI-digested pF3A using the GeneArt Seamless cloning and assembly kit (Invitrogen) according to the manufacturer's instructions and then sequence-verified. Cell-free expression was conducted with a wheat germ coupled transcription/translation kit (Promega) driven by the T7 promoter of pF3A. In vitro protein synthesis was performed according to the manufacturer's instructions, including optimization steps involving test reactions with titrations of DNA and various additives. From the conditions tested, optimal synthesis was obtained with the addition of 0.1 mM cellobiose, with DNA concentrations of 30 to 45 µg/mL and a reaction time of 4 h at room temperature, and proteins were labeled by the addition of 1175 Ci/mmol [^{35}S]methionine (Perkin-Elmer; NEG709A). To remove endogenous wheat germ proteins that cross-reacted with CESA antibodies, completed translation reactions were brought to 25% ammonium sulfate saturation, incubated for 10 min at room temperature, and centrifuged for 15 min at 13,000*g* in a microcentrifuge. The supernatant of the ammonium sulfate precipitation was used for CESA4 and CESA8, whereas the pellet fraction was used for CESA7. After ammonium sulfate precipitation, unincorporated ^{35}S was removed by a trichloroacetic acid precipitation and chloroform extraction (Wang et al., 2006b); the resulting protein pellet was then resuspended in SDS-PAGE loading buffer (Laemmli, 1970), divided into aliquots, and frozen until SDS-PAGE analysis.

Plants and Growth Conditions

Seeds were obtained from the ABRC: wild-type *Arabidopsis* of the Columbia ecotype (CS70000) and *cesa* knockout mutants in the Columbia background, CESA4 ko (*irx5-4*; SALK_084627), CESA7 ko (*irx3-4*; SALK_029940C), and CESA8 ko (*irx1-5*; SALK_026812C) (Alonso et al.,

2003). Plants were grown at 22 to 24°C with 18-h days. A biological insecticide (Dr. Pye's Scanmask; Hirt's Gardens) was used to control fungus gnats.

Protein Extraction from *Arabidopsis*

Stems were harvested from 6- to 7-week-old plants, siliques and leaves were removed, and the stems were immediately ground to a fine powder in liquid nitrogen. For stoichiometry determination, only the region corresponding to ~50 to 75% of the stem length was used from a pool of 30 to 50 plants. For the analysis of knockout lines, the entire stem was used. For stem sectioning, the indicated region was used from a pool of 10 plants. The N_2-ground powder was resuspended in acetone containing 10% trichloroacetic acid, and total protein was extracted (Wang et al., 2006b). Final protein pellets were resuspended in dilute phosphate-buffered saline containing 1% SDS. Protein concentration was assayed by a modified Lowry procedure (Peterson, 1977). Samples for quantitative immunoblotting were diluted to 1 mg/mL into SDS-PAGE loading buffer, divided into aliquots, frozen in liquid nitrogen, and stored at −80°C until SDS-PAGE analysis. Samples for the analysis of knockout lines and stem sectioning were diluted to ~2.5 mg/mL with phosphate-buffered saline containing 1% SDS, and then a second Lowry procedure was performed to ensure accuracy. Samples were then diluted to exactly 2 mg/mL into SDS-PAGE loading buffer, divided into aliquots, and frozen until analysis.

Quantitative Immunoblotting

A series of ^{35}S-labeled CESA standards and total stem protein was separated on 8% SDS-PAGE gels with a 5% stacking gel (pH 8.8, with 35% glycerol), transferred to 0.1-μm pore nitrocellulose (Whatman), and then dried. Blots were blocked in Tris-buffered saline (TBS) containing 0.5% Tween 20. Washes, primary antibody, and secondary antibody (goat anti-rabbit horseradish peroxidase conjugate; KPL 95058-730) dilutions were in TBS containing 0.25% Tween 20. Blots were developed using SuperSignal West Pico Chemiluminescent Substrate (Thermo) and visualized by exposure to CL-Xposure Film (Thermo). Films were digitized and intensity was quantified by ImageJ software (National Institutes of Health). After exposure to x-ray film, immunoblots were washed in TBS briefly and then developed with the colorimetric chloronaphthol/diaminobenzidine reagent (Thermo). Bands of the ^{35}S standard were excised, dissolved in FilterCount (Perkin-Elmer), and quantified by liquid scintillation counting with an internal standard. Molar amount was determined by multiplying the amount of methionine in the internal standard (9360 amol) by the cpm ratio of the sample to the internal standard (9360 × sample cpm/standard cpm). This provided the molar amount of methionines in the sample, which was divided by the number of methionines in each CESA (CESA4, 22; CESA7, 28; and CESA8, 19) to determine the mole amount of CESA within each band of the standard curve. Each immunoblot contains both a standard curve and a series of stem protein samples. For each, a standard curve was created by plotting the molar amount of the CESA versus band intensity. The equation from this curve was then used to convert band intensity from the series of stem protein samples to amol CESA/μg total protein.

Stem Sectioning and Immunoblotting

Arabidopsis stems were harvested at 6 weeks. Leaves, branches, and siliques were gently removed, and the length was measured. Nine sections corresponding to 10% of the total length were cut, starting at 5% and ending at 95%, and immediately frozen in liquid nitrogen. Sections from 10 stems were pooled and ground in liquid nitrogen. Protein was prepared and sample concentration was normalized to total protein amount as per the protein extraction section above. Equal amounts of protein were separated by SDS-PAGE and immunoblotted, and band intensities were measured as in the quantitative immunoblotting methods above. A single section was chosen, and for each CESA, all points were normalized to the band intensity values of that point.

Accession Numbers

Accession numbers for CESA1, CESA3, CESA6, CESA4, CESA7, and CESA8 cDNA are NM_119393, NM_120599, NM_125870, NM_123770, NM_121748, and NM_117994, respectively. The Arabidopsis Genome Initiative identifiers for CESA1, CESA3, CESA6, CESA4, CESA7, and CESA8 are AT4G32410, AT5G05170, AT5G64740, AT5G44030, AT5G17420, and AT4G18780, respectively.

Supplemental Data

The following materials are available in the online version of this article.

Supplemental Figure 1. Multiple Sequence Alignment of CESAs with Epitope Peptides Highlighted.

Supplemental Table 1. Peptides Used to Generate CESA Antibodies.

Supplemental Table 2. Primers for Cloning of CESAs into pF3A.

ACKNOWLEDGMENTS

This work was supported by the Center for LignoCellulose Structure and Formation, an Energy Frontier Research Center funded by the U.S. Department of Energy, Office of Science, Office of Basic Energy Sciences, under Grant DE-SC0001090.

AUTHOR CONTRIBUTIONS

J.L.H. and M.T. designed the research. J.L.H. and M.B.H. performed research. J.L.H. and M.T. analyzed data and wrote the article.

Received August 19, 2014; revised November 17, 2014; accepted November 20, 2014; published December 9, 2014.

REFERENCES

Alonso, J.M., et al. (2003). Genome-wide insertional mutagenesis of *Arabidopsis thaliana*. Science **301:** 653–657.

Atanassov, I.I., Pittman, J.K., and Turner, S.R. (2009). Elucidating the mechanisms of assembly and subunit interaction of the cellulose synthase complex of Arabidopsis secondary cell walls. J. Biol. Chem. **284:** 3833–3841.

Bashline, L., Li, S., Anderson, C.T., Lei, L., and Gu, Y. (2013). The endocytosis of cellulose synthase in Arabidopsis is dependent on μ2, a clathrin-mediated endocytosis adaptin. Plant Physiol. **163:** 150–160.

Brown, D.M., Zeef, L.A.H., Ellis, J., Goodacre, R., and Turner, S.R. (2005). Identification of novel genes in *Arabidopsis* involved in secondary cell wall formation using expression profiling and reverse genetics. Plant Cell **17:** 2281–2295.

Brown, R.M., Jr., Willison, J.H., and Richardson, C.L. (1976). Cellulose biosynthesis in Acetobacter xylinum: Visualization of the site of synthesis and direct measurement of the in vivo process. Proc. Natl. Acad. Sci. USA **73:** 4565–4569.

Carpita, N.C. (2011). Update on mechanisms of plant cell wall biosynthesis: How plants make cellulose and other (1→4)-β-D-glycans. Plant Physiol. **155:** 171–184.

Carroll, A., and Specht, C.D. (2011). Understanding plant cellulose synthases through a comprehensive investigation of the cellulose synthase family sequences. Front. Plant Sci. **2:** 5.

Carroll, A., Mansoori, N., Li, S., Lei, L., Vernhettes, S., Visser, R.G.F., Somerville, C., Gu, Y., and Trindade, L.M. (2012). Complexes with mixed primary and secondary cellulose synthases are functional in Arabidopsis plants. Plant Physiol. **160:** 726–737.

Chanzy, H., Imada, K., Mollard, A., Vuong, R., and Barnoud, F. (1979). Crystallographic aspects of sub-elementary cellulose fibrils occurring in the wall of rose cells cultured in vitro. Protoplasma **100:** 303–316.

Chanzy, H., Imada, K., and Vuong, R. (1978). Electron diffraction from the primary wall of cotton fibers. Protoplasma **94:** 299–306.

Desprez, T., Juraniec, M., Crowell, E.F., Jouy, H., Pochylova, Z., Parcy, F., Höfte, H., Gonneau, M., and Vernhettes, S. (2007). Organization of cellulose synthase complexes involved in primary cell wall synthesis in *Arabidopsis thaliana*. Proc. Natl. Acad. Sci. USA **104:** 15572–15577.

Doblin, M.S., Kurek, I., Jacob-Wilk, D., and Delmer, D.P. (2002). Cellulose biosynthesis in plants: From genes to rosettes. Plant Cell Physiol. **43:** 1407–1420.

Fernandes, A.N., Thomas, L.H., Altaner, C.M., Callow, P., Forsyth, V.T., Apperley, D.C., Kennedy, C.J., and Jarvis, M.C. (2011). Nanostructure of cellulose microfibrils in spruce wood. Proc. Natl. Acad. Sci. USA **108:** E1195–E1203.

Gardiner, J.C., Taylor, N.G., and Turner, S.R. (2003). Control of cellulose synthase complex localization in developing xylem. Plant Cell **15:** 1740–1748.

Gu, Y., Kaplinsky, N., Bringmann, M., Cobb, A., Carroll, A., Sampathkumar, A., Baskin, T.I., Persson, S., and Somerville, C.R. (2010). Identification of a cellulose synthase-associated protein required for cellulose biosynthesis. Proc. Natl. Acad. Sci. USA **107:** 12866–12871.

Guerriero, G., Fugelstad, J., and Bulone, V. (2010). What do we really know about cellulose biosynthesis in higher plants? J. Integr. Plant Biol. **52:** 161–175.

Ha, M.A., Apperley, D.C., Evans, B.W., Huxham, I.M., Jardine, W.G., Viëtor, R.J., Reis, D., Vian, B., and Jarvis, M.C. (1998). Fine structure in cellulose microfibrils: NMR evidence from onion and quince. Plant J. **16:** 183–190.

Ha, M.-A., MacKinnon, I.M., Sturcová, A., Apperley, D.C., McCann, M.C., Turner, S.R., and Jarvis, M.C. (2002). Structure of cellulose-deficient secondary cell walls from the irx3 mutant of *Arabidopsis thaliana*. Phytochemistry **61:** 7–14.

Herth, W. (1983). Arrays of plasma-membrane "rosettes" involved in cellulose microfibril formation of *Spirogyra*. Planta **159:** 347–356.

Kennedy, C.J., Cameron, G.J., Šturcová, A., Apperley, D.C., Altaner, C., Wess, T.J., and Jarvis, M.C. (2007). Microfibril diameter in celery collenchyma cellulose: X-ray scattering and NMR evidence. Cellulose **14:** 235–246.

Kimura, S., Laosinchai, W., Itoh, T., Cui, X., Linder, C.R., and Brown, R.M., Jr. (1999). Immunogold labeling of rosette terminal cellulose-synthesizing complexes in the vascular plant *Vigna angularis*. Plant Cell **11:** 2075–2086.

Laemmli, U.K. (1970). Cleavage of structural proteins during the assembly of the head of bacteriophage T4. Nature **227:** 680–685.

Li, S., Lei, L., and Gu, Y. (2013). Functional analysis of complexes with mixed primary and secondary cellulose synthases. Plant Signal. Behav. **8:** e23179.

Morgan, J.L.W., Strumillo, J., and Zimmer, J. (2013). Crystallographic snapshot of cellulose synthesis and membrane translocation. Nature **493:** 181–186.

Mueller, S.C., and Brown, R.M., Jr. (1980). Evidence for an intramembrane component associated with a cellulose microfibril-synthesizing complex in higher plants. J. Cell Biol. **84:** 315–326.

Newman, R.H., Hill, S.J., and Harris, P.J. (2013). Wide-angle x-ray scattering and solid-state nuclear magnetic resonance data combined to test models for cellulose microfibrils in mung bean cell walls. Plant Physiol. **163:** 1558–1567.

Olek, A.T., et al. (2014). The structure of the catalytic domain of a plant cellulose synthase and its assembly into dimers. Plant Cell **26:** 2996–3009.

Persson, S., Paredez, A., Carroll, A., Palsdottir, H., Doblin, M., Poindexter, P., Khitrov, N., Auer, M., and Somerville, C.R. (2007). Genetic evidence for three unique components in primary cell-wall cellulose synthase complexes in Arabidopsis. Proc. Natl. Acad. Sci. USA **104:** 15566–15571.

Peterson, G.L. (1977). A simplification of the protein assay method of Lowry et al. which is more generally applicable. Anal. Biochem. **83:** 346–356.

Schneider, C.A., Rasband, W.S., and Eliceiri, K.W. (2012). NIH Image to ImageJ: 25 years of image analysis. Nat. Methods **9:** 671–675.

Sethaphong, L., Haigler, C.H., Kubicki, J.D., Zimmer, J., Bonetta, D., DeBolt, S., and Yingling, Y.G. (2013). Tertiary model of a plant cellulose synthase. Proc. Natl. Acad. Sci. USA **110:** 7512–7517.

Taylor, N.G. (2008). Cellulose biosynthesis and deposition in higher plants. New Phytol. **178:** 239–252.

Taylor, N.G., Howells, R.M., Huttly, A.K., Vickers, K., and Turner, S.R. (2003). Interactions among three distinct CesA proteins essential for cellulose synthesis. Proc. Natl. Acad. Sci. USA **100:** 1450–1455.

Thimm, J.C., Burritt, D.J., Sims, I.M., Newman, R.H., Ducker, W.A., and Melton, L.D. (2002). Celery (*Apium graveolens*) parenchyma cell walls: Cell walls with minimal xyloglucan. Physiol. Plant. **116:** 164–171.

Thomas, L.H., Forsyth, V.T., Sturcová, A., Kennedy, C.J., May, R.P., Altaner, C.M., Apperley, D.C., Wess, T.J., and Jarvis, M.C. (2013). Structure of cellulose microfibrils in primary cell walls from collenchyma. Plant Physiol. **161:** 465–476.

Timmers, J., Vernhettes, S., Desprez, T., Vincken, J.-P., Visser, R.G.F., and Trindade, L.M. (2009). Interactions between membrane-bound cellulose synthases involved in the synthesis of the secondary cell wall. FEBS Lett. **583:** 978–982.

Vain, T., Crowell, E.F., Timpano, H., Biot, E., Desprez, T., Mansoori, N., Trindade, L.M., Pagant, S., Robert, S., Höfte, H., Gonneau, M., and Vernhettes, S. (2014). The cellulase KORRIGAN is part of the cellulose synthase complex. Plant Physiol. **165:** 1521–1532.

Visakh, P.M., and Thomas, S. (2010). Preparation of bionanomaterials and their polymer nanocomposites from waste and biomass. Waste and Biomass Valorization **1:** 121–134.

Wang, J., Elliott, J.E., and Williamson, R.E. (2008). Features of the primary wall CESA complex in wild type and cellulose-deficient mutants of *Arabidopsis thaliana*. J. Exp. Bot. **59:** 2627–2637.

Wang, J., Howles, P.A., Cork, A.H., Birch, R.J., and Williamson, R.E. (2006a). Chimeric proteins suggest that the catalytic and/or C-terminal domains give CesA1 and CesA3 access to their specific sites in the cellulose synthase of primary walls. Plant Physiol. **142:** 685–695.

Wang, W., Vignani, R., Scali, M., and Cresti, M. (2006b). A universal and rapid protocol for protein extraction from recalcitrant plant tissues for proteomic analysis. Electrophoresis **27:** 2782–2786.

Wittig, I., Beckhaus, T., Wumaier, Z., Karas, M., and Schägger, H. (2010). Mass estimation of native proteins by blue native electrophoresis: Principles and practical hints. Mol. Cell. Proteomics **9:** 2149–2161.